Solid-State Structures of Three Zinc(II) Coordination Polymers with 3-(1H-Imidazol-1-yl)propanoate Linkers Prepared in Water

Katharina Kodolitsch, Ana Torvisco, Tomas Kamencek, Matjaž Mazaj, Egbert Zojer, and Christian Slugovc*

Coordination polymers of zinc(II) with three readily accessible 3-(1H-imidazol-1-yl)propanoate ligands are prepared by combining aqueous solutions of the ligands and zinc(II) salts, resulting in a precipitation of the respective coordination polymers. While sodium 3-(1H-imidazol-1-yl)propanoate and sodium 3-(2-phenyl-1H-imidazol-1-yl)propanoate initially yield amorphous precipitates that can be converted to crystalline materials upon prolonged heating, the use of sodium 3-(2-methyl-1H-imidazol-1-yl)propanoate results in the immediate formation of a crystalline

coordination polymer. All three coordination polymers are structurally characterized by single-crystal X-ray diffraction. The crystal water in one coordination polymer can be removed without losing the crystallinity of the sample and this process is studied by infrared spectroscopy. The interpretation of the corresponding infrared spectra is supported by theoretical calculations. Furthermore, the solubility in water and buffer solutions and the potential porosity of the coordination polymers are investigated, revealing their nonporous character for CO_2, N_2, and CH_4.

1. Introduction

Metal-organic frameworks (MOFs) have received tremendous attention in recent years, not only because of their remarkable structures and diverse topologies, but also because of their interesting properties and potential applications. These comprise gas storage, adsorption-based gas/vapor separation, shape/size-selective catalysis, or applications in the biomedical field.[1–3] In the latter case, metal ions such as Zn^{2+}, which have no or low toxicity, are preferred.[4] Zinc ions are the metal nodes in two prominent MOF classes, the IRMOF series composed of Zn_4O

inorganic clusters linked by aromatic dicarboxylates such as tere-phthalate in IRMOF-1 (MOF-5),[5] and the ZIF class composed of Zn^{2+} ions connected by four imidazolate ligands resulting in a tetrahedral coordination geometry around the metals.[6] While the ZIF class is water tolerant,[7,8] another important requirement for many applications, the IRMOF class is not. This is a consequence of the hydrolytic instability of the Zn_4O clusters used as secondary building blocks.[9,10] Compared to these two large classes of MOFs, Zn^{2+}-based organic frameworks containing carboxylate and nitrogen donor type ligands in the structure have received less attention, probably because of the significantly increased structural diversity of this class of materials, which generally have low surface areas.[11,12] Examples of Zn^{2+}-based MOFs built using ditopic linkers containing a carboxylate and a nitrogen donor in the same molecule are more rare. This is probably because of the significantly higher synthetic effort required to prepare such linkers. **Figure 1** shows the linkers combining an N-donor and a carboxylate group in the same molecule used to prepare Zn^{2+} organic frameworks. Only the linkers A[13] and D[14] combine a carboxylate and a neutral N-donor ligand in the same molecule. Ligands B,[15] C,[16] and E[17] provide additional N-donor binding sites.

In addition, linkers have been used that combine two or more carboxylate groups with N-donor binding sites.[18–24] Most of the resulting Zn^{2+} materials were prepared from water-dimethylformamid mixtures or from pure water and in most cases can be regarded as 1D or 2D-coordination polymers.

Here, we disclose a water-soluble and flexible linker family, which is prepared by a facile, solvent and catalyst-free route.[25] These linkers are then used in the synthesis of Zn^{2+}-based coordination polymers in aqueous solution. The resulting materials are structurally characterized and their thermal stability, porosity, and solubility in water were investigated.

K. Kodolitsch, C. Slugovc
Institute for Chemistry and Technology of Materials (ICTM)
Graz University of Technology
Stremayrgasse 9, 8010 Graz, Austria
E-mail: slugovc@tugraz.at

A. Torvisco
Institute of Inorganic Chemistry
NAWI Graz
Graz University of Technology
Stremayrgasse 9, 8010 Graz, Austria

T. Kamencek, E. Zojer
Institute of Solid-State Physics
NAWI Graz
Graz University of Technology
Petersgasse 16/II, 8010 Graz, Austria

M. Mazaj
Department of Inorganic Chemistry and Technology
National Institute of Chemistry
Hajdrihova 19, Ljubljana 1001, Slovenia

C. Slugovc
Christian Doppler Laboratory for Organocatalysis in Polymerization
Stremayrgasse 9, 8010 Graz, Austria

EurJIC
European Journal of Inorganic Chemistry

Research Article
doi.org/10.1002/ejic.202500032

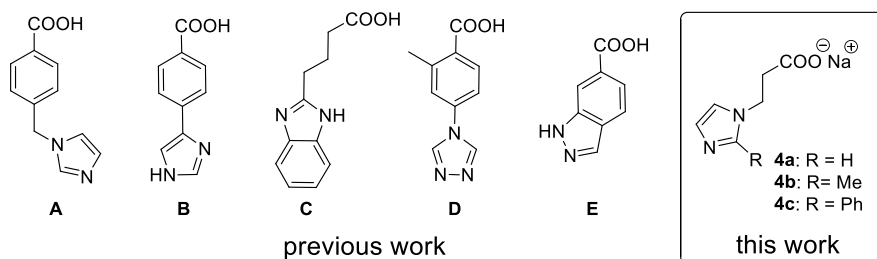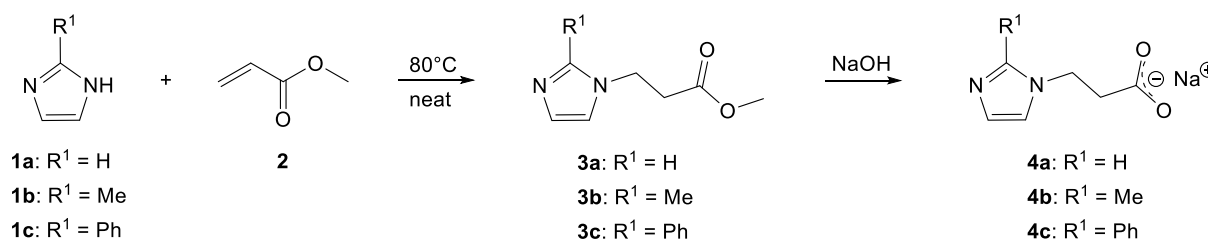**Chemistry Europe**
European Chemical Societies Publishing

Figure 1. N,O-donor ligands previously used to prepare Zn^{2+} coordination polymers and the linker introduced in this work (boxed in).

2. Results and Discussion

The linker molecules used in this work were prepared in a two-step reaction sequence (see **Scheme 1**) starting from the corresponding imidazole derivatives (**1a–c**) and methyl acrylate (**2**). In the first step, an aza-Michael reaction is performed using a recently disclosed catalyst and a solvent-free protocol which provides virtually quantitative yields of the alkyl propanoates **3a–c**.[26] Subsequent saponification was accomplished by adding 1.03 eq. aqueous NaOH to the corresponding methyl propanoates **3a–c** and placing the open reaction vessel in an oven at 80 °C. This yielded the corresponding analytically pure products in virtually quantitative yields after drying. All linker variants of the sodium propanoate family **4a–c** are, as expected, water soluble.

The linkers **4a–c** were then used to coordinate Zn^{2+} ions in aqueous solution. $Zn(NO_3)_2 \cdot 6\,H_2O$ was used as the source for the metal ion. Solutions of the linker ($c = 0.1\,mol\,L^{-1}$) and the Zn salt ($c = 0.5\,mol\,L^{-1}$) were prepared and the latter was slowly added dropwise to the linker solution at room temperature. When **4a** was used as linker, an amorphous oily layer formed at the bottom of the reaction vessel after a few minutes. After a certain time (sometimes hours, sometimes days), almost all of the oil was converted into colorless to light yellow crystals suitable for single crystal X-ray structure determination (sc-XRD) measurements. The crystals named GUT1 (for Graz University of Technology) crystallize in the space group $Pca2_1$ and contained 4 Zn atoms in the unit cell. The coordination geometry of the zinc atoms is tetrahedral and each Zn atom is connected to two imidazole nitrogens and two carboxylate groups of four different linkers in κ^1-fashion. Each linker **4a** bridges two different metal atoms, forming a 2D network of 32-membered rings connected via four Zn-atoms (**Figure 2**).
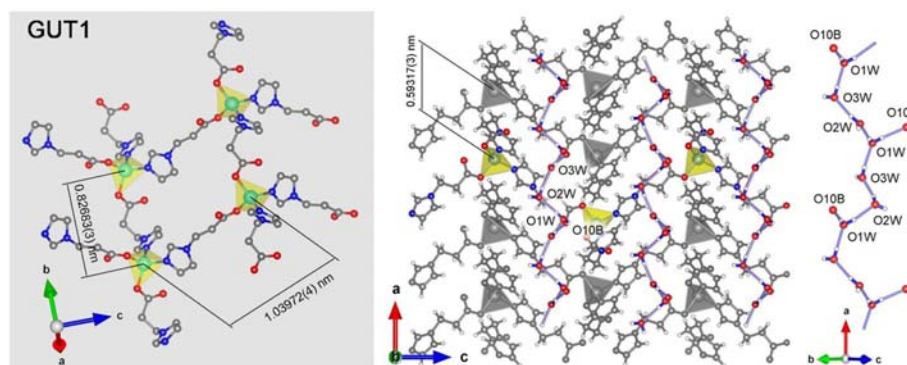

Scheme 1. Linker synthesis.

Figure 2. Left panel: repeating unit of the 2D coordination polymer GUT1 showing the 32 membered ring system (hydrogens and water omitted for clarity); the smallest Zn-Zn intra sheet distances are 8.2687(3) Å and 10.3972(4) Å, respectively; center panel: view of the crystal along the *b*-axis showing the smallest Zn-Zn inter-sheet distance of 5.9317(3) Å and the 2D-coordination-polymer sheets kinked by 114.412(5)° and their assembly held together by hydrogen bonds between carbonyl oxygen atoms (O10B) of the ligands and every third water molecule (O1W) from infinite water chains (involving three independent water molecules O1W-O3W); rightmost panel: water needles with the 2D coordination polymer knocked out (except O10B). Visualization performed using VESTA.[58]

Eur. J. Inorg. Chem. **2025**, 28, e202500032 (2 of 10)

© 2025 Wiley-VCH GmbH

EurJIC
European Journal of Inorganic Chemistry

Research Article
doi.org/10.1002/ejic.202500032

Chemistry
Europe
European Chemical
Societies Publishing

The 2D network is bent by an angle of 114.412(5)° and the network sheets are stacked to form a herringbone pattern when viewed along the *b*-axis (see Figure 2 center panel). A similar 2D network arrangement was formed in the solid state when Zn^{2+} and ligand A (from Figure 1) were used.[13] In GUT1, so-called water needles,[27] formed by hydrogen bonding of three crystallographically independent water molecules located in the vacancies of the crystal structure, connect the 2D network sheets to form a 3D network. This is achieved via a hydrogen bonding interaction of every third water molecule with carbonyl oxygen (O1B) of a linker with the biggest channel extending along the *a*-axis (area of the shamrock-like cross section would be about 10 Å²) (Figure 2). Porosity in GUT1 is largely blocked by the water needles (**Figure 3**). Removal of the water could potentially release channels throughout the crystal. However, upon drying in a vacuum, crystals turn opaque and the crystallinity is lost as revealed by p-XRD measurements (Figure 3).

The use of the 2-methylimidazole-based linker **4b** instead of **4a** resulted in the immediate formation of a turbid solution directly followed by the precipitation of a crystalline material, provided that relatively concentrated precursor solutions are used ([**4b**] = 0.156 mol L⁻¹, [Zn^{2+}] = 0.079 mol L⁻¹). After standing at room temperature for 24 h, colorless crystals suitable for sc-XRD measurements were obtained. The compound designated GUT2 crystallized in the space group *Pcca* with 8 Zn atoms in the unit cell. Tetrahedral zinc coordination with two imidazole nitrogen atoms and two carboxylate groups in κ¹-fashion is observed.

The linkage between two zinc atoms is established by two bridging ligands **4b** that form 16-membered rings in such a way that both linkers point in the same direction (i.e., within a macrocycle, one zinc atom coordinates to two imidazole nitrogen atoms and the other to two carboxylate ligands). Individual polymer chains alternate along the *b*-axis of the crystal (**Figure 4**, left) and are held together by hydrogen bonds in the c-direction of the unit cell. These occur between one of the carbonyl oxygens (O1A), an additional water molecule (O1W), and the carbonyl oxygen (O1B) of the neighboring coordination polymer (Figure 4). In contrast to GUT1, the crystal water in GUT2 only blocks the relatively small channels along the *b*-axis. The larger channels along the *a*- and *c*-axes (cross-sectional area of about 9 Å²) are not affected and remain accessible (**Figure 5**). In addition, the crystallinity of GUT2 is not lost upon drying, as shown by p-XRD measurements (Figure 5).

The use of the 2-phenylimidazole-based linker **4c** immediately produced an amorphous, voluminous white precipitate (**Figure 6**). Upon heating to 80 °C, the cloudy precipitate contracted and transformed into a microcrystalline material. By partially dissolving the microcrystalline material at 120 °C in water (in a pressure vessel), separating the supernatant solution at room temperature, and placing this solution in an oven at 80 °C for several days, crystals large enough for sc-XRD measurements were obtained. These revealed that GUT3 crystallizes in the space group P 2/n and is, beside this, structurally very similar to GUT2, i.e., 1D coordination polymers are formed in the solid state in an
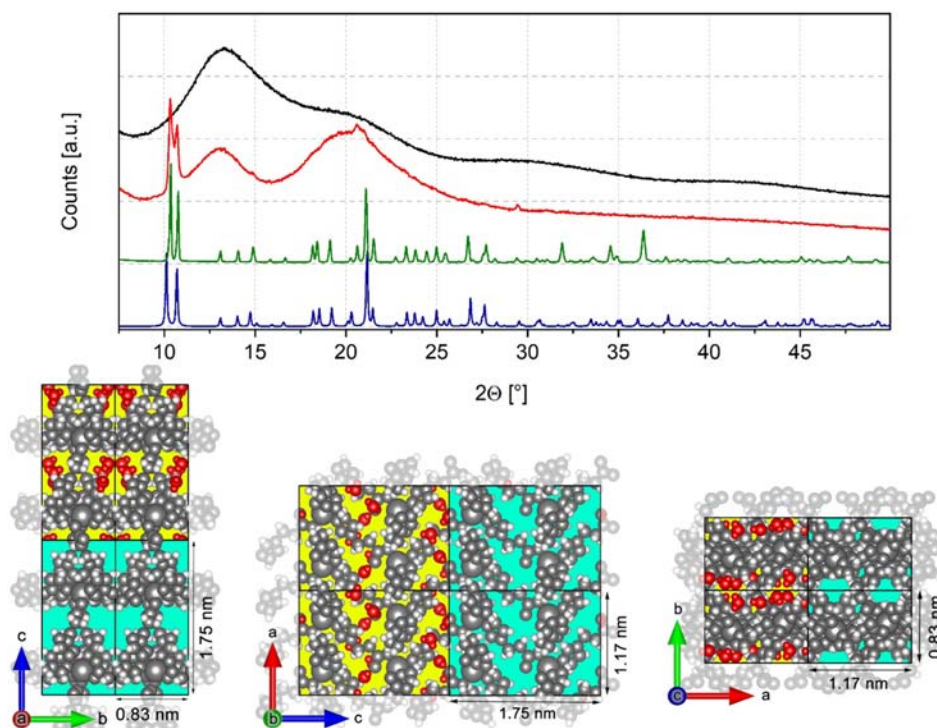

Figure 3. Above: p-XRD of GUT1; blue: calculated from the structure identified via sc-XRD data; green: measured from single crystals; red: measured after drying of single crystals; black: measurement of the initial precipitate. Below: Space fill model of four elemental cells of GUT1 (C, N, O, Zn shown in gray, H shown in white) seen along the *a*, *b*, and *c* axes visualizing water (O and H in red) enclosed in the structure and the resulting void space (colored in yellow) and visualizing the hypothetical structure obtained after removal of the water molecules (void space in turquoise). The dimensions of the unit cell are specified. Visualization was done using VESTA.[58]
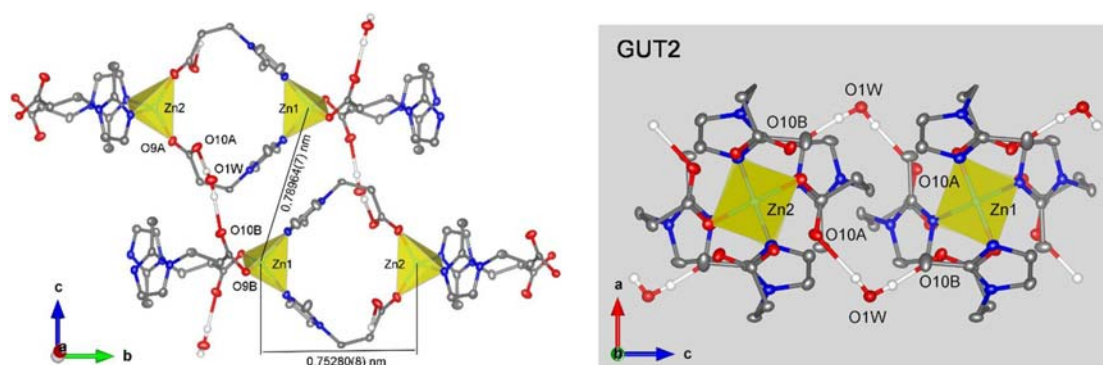
EurJIC
European Journal of Inorganic Chemistry

Research Article
doi.org/10.1002/ejic.202500032

Chemistry
Europe
European Chemical
Societies Publishing

Figure 4. Sections of two neighboring 1D coordination polymers showing the 16 ring system (hydrogens except for crystal water omitted for clarity, Zn-Zn distance within a chain is 7.5280(8) Å) and their alternating direction as well as the hydrogen bonding via a water molecule (O1W) connecting the chains (smallest Zn-Zn interchain distance is 7.8964(7) Å); left: view along the *a*-axis; right: view along the *b*-axis. Visualization was done with the aid of VESTA.[58]
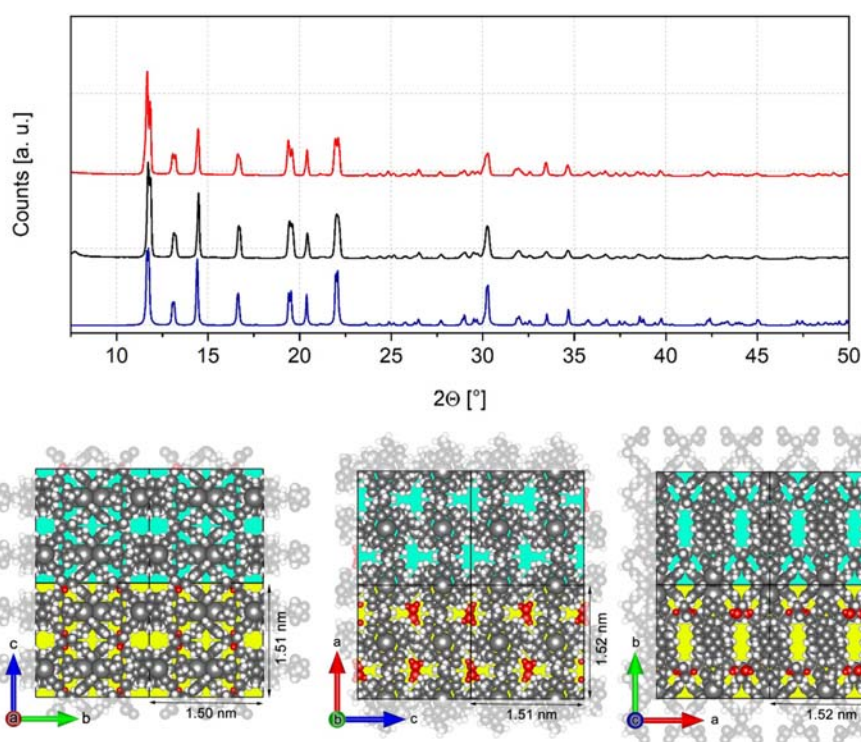

Figure 5. Above: p-XRD of GUT2; blue: calculated from sc-XRD data; black: measurement of the initial precipitate; red: measured after drying of single crystals. Below: Space fill model of four elemental cells of GUT2 (C, N, O, Zn shown in gray, H shown in white) seen along the *a*, *b*, and *c* axes visualizing water enclosed in the structure (O and H in red) and the resulting void space (colored in yellow) and visualizing the hypothetical structure after removal of the water molecules (void space in turquoise). Dimensions of the elemental cell are given. Visualization was done with the aid of VESTA.[58]

arrangement similar to GUT2 (Figure 6). However, the disorder of half of the phenyl rings in the structure does not allow a detailed discussion of the structural features.

The thermal stability of the coordination polymers was accessed by thermogravimetric analysis (TGA). For this purpose, two types of samples, namely wet and dried samples, were prepared. The wet samples were obtained by isolating the precipitate by filtration and drying the obtained solids for 1 h at a pressure of 20 mbar at room temperature. Dried samples were obtained by drying the solids for 8 h at a pressure of 3 mbar at 50 °C. In the case of GUT1, the drying conditions chosen were

not suitable for the complete removal of the crystal water, as the analysis of dried GUT1 shows a mass loss of 7.8 w% (corresponding to approx. 1.7 eq. water) up to a temperature of 110 °C (solid red line in **Figure 7**). Notably, the wet GUT1 sample shows only a somewhat larger mass loss of 10.2 w% (about 2.3 eq. water) in the same temperature range. No further mass loss was detected from 110 °C to about 230 °C for both samples. At higher temperatures, decomposition started and a small endothermic signal was detected at 233 °C in the simultaneously performed differential scanning calorimetry (DSC) experiment (see dotted red line in Figure 7). Wet GUT2 loses ≈1 eq. water (4.7 w%) up to a
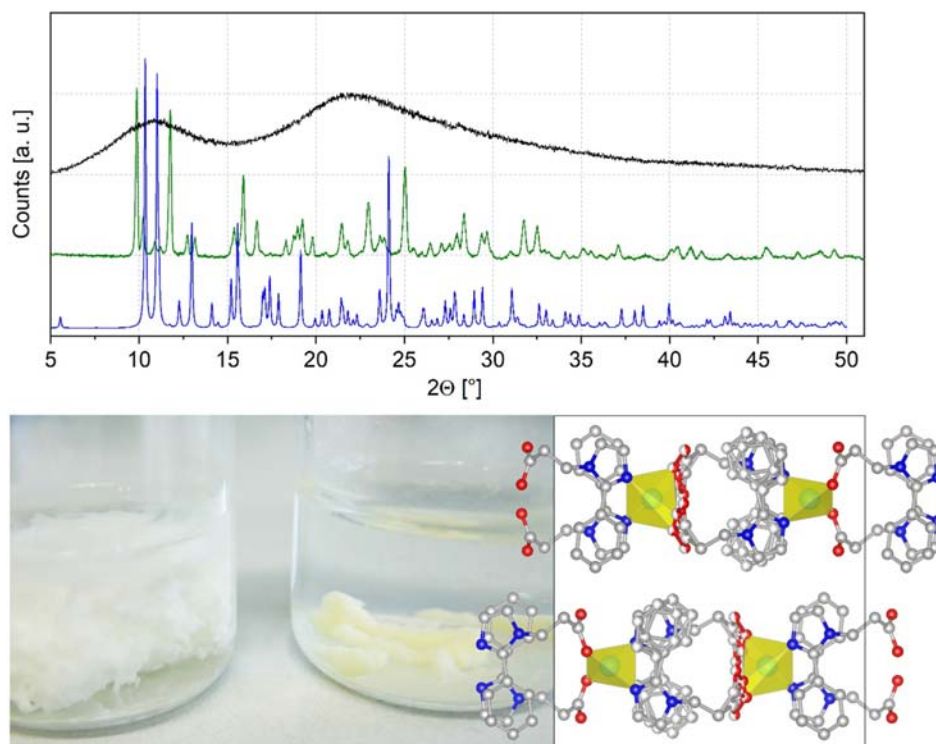
Eur. J. Inorg. Chem. **2025**, *28*, e202500032 (4 of 10)

© 2025 Wiley-VCH GmbH

Figure 6. Left: p-XRD of GUT3; blue: calculated from sc-XRD data; green: measured from single crystals; black: measurement of the initial precipitate. Right above: Photograph of the initial and aged precipitate of GUT3. Right below: unit cell of GUT3 seen along the *a*-axis. Visualization was done with the aid of VESTA.[58]

temperature of about 112 °C. In contrast, dried GUT2 shows no mass loss up to about 270 °C. A rather broad endothermic signal is observed in the DSC, peaking at 295 °C, which is consistent with rapid mass loss observed in the TGA experiment and which again indicates a disintegration of the sample. In GUT3, wet and dried samples showed very similar TGA results with no mass loss up to a

temperature of about 210 °C. The DSC showed an endothermic heat flux peaking at 248 °C.

Notably, the thermal stability of ligands **4a–c** is similar (Figure S12, Supporting Information) and, thus, the moderate thermal stability of the investigated coordination polymers can be primarily attributed to the linkers. In fact, MOF-5 (400–500 °C)[28] and ZIF-8 (about 500 °C; heating rate of 10 °C min^{-1} under N$_2$)[29] feature higher decomposition temperatures under similar experimental conditions. The data in Figure 7 also show that crystal water can be easily removed from GUT1 and GUT2 and does not seem to be present in GUT3. Accordingly, channels in GUT1 and GUT2 are suitable to transport water (with a kinetic diameter of 2.65 Å) out of the crystals.

The presence and absence of water were further investigated by ATR-IR spectroscopy and spectra calculated based on the sc-XRD unit cells were used to assign the observed absorptions to atomic motions. For this purpose, crystalline samples of GUT1 and GUT2 were measured in wet and dry states (72 h at a pressure of 3 mbar at 50 °C) and simulated in the wet case. In the following, the simulated spectra, which showed good agreement with the measured spectra, are discussed, as the animations of the associated vibrational modes allow an explanation of the nature of the atomic motions. In passing, it is noted that simulated and measured peak intensities are not expected to necessarily agree for reasons mentioned in the Experimental Section and discussed in more detail in the Supporting Information. Starting with GUT1, the strongest peak (1588 cm^{-1}, labeled as Roman number I in **Figure 8**) corresponds to asymmetric stretching in the COO$^-$
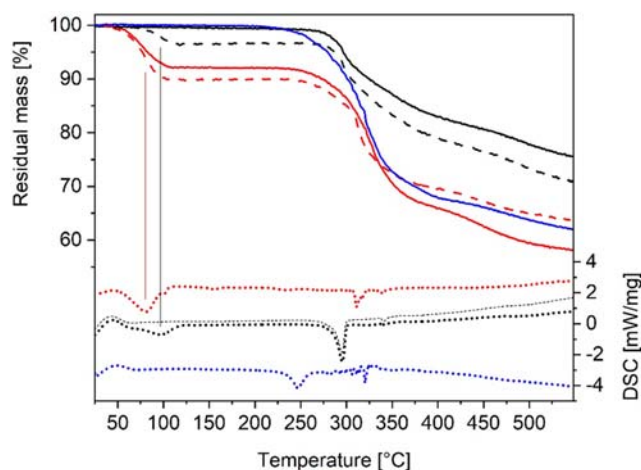

Figure 7. Thermogravimetry for GUT1 (red) in its dried state (full line) and in its wet state (dashed line). The equivalent data for GUT2 are shown as solid and dashed black lines. For GUT3, only a single blue curve is shown, as wet and dry samples gave the same result. DSC data are shown in the bottom part of the plot as dotted curves using the same color code. Both data were acquired with a heating rate of 10 °C min^{-1} under N$_2$.

Eur. J. Inorg. Chem. **2025**, *28*, e202500032 (5 of 10)

© 2025 Wiley-VCH GmbH

EurJIC
European Journal of Inorganic Chemistry

Research Article
doi.org/10.1002/ejic.202500032

Chemistry
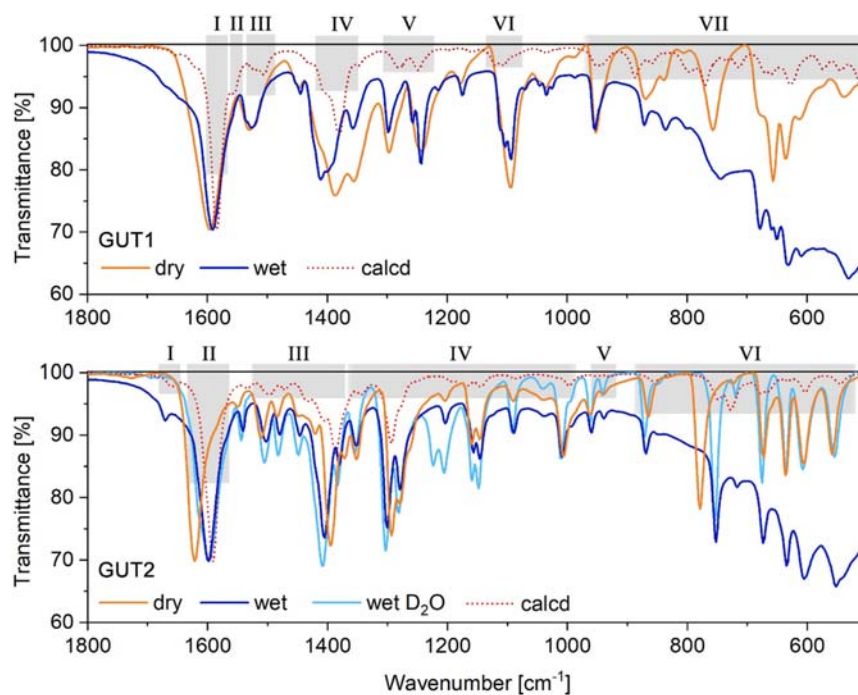**Europe**
European Chemical
Societies Publishing

Figure 8. IR spectra for GUT1 and GUT2 measured in the dried and wet state and calculated for the wet state. For GUT2, also the spectrum for a sample grown from D_2O solution is shown.

moiety with a minor contribution of crystal water. The water contribution becomes stronger for slightly lower wavenumbers (1556 cm^{-1}, region II). There, one can observe strong O—H bending in the crystal water molecules. The next lower peaks (region III) correspond to in-plane deformations in the imidazolate moieties (1525–1518 cm^{-1}). In region IV, several (similar) vibrational modes are distributed over a relatively large frequency range. All of them involve C—H bending in the CH_2 moieties of the linkers (1431–1347 cm^{-1}). Region V essentially comprises modes, which involve combinations of in-plane bending of the imidazolate (as in region III) and the aforementioned C—H bending (as in region IV) (1276–1247 cm^{-1}). Region VI is characterized by in-plane bending of the hydrogens of the imidazolate moieties, with the small peak at ≈1032 cm^{-1} also showing torsional distortions in the aliphatic parts of the linkers (1120–1032 cm^{-1}). In region VII, one can observe mainly three types of motions, which are combined to different extents. The motions are out-of-plane bending, distortions of imidazolates, and rotations of the crystal water (<952 cm^{-1}). Only the IR active mode at ≈672 cm^{-1} is slightly different in nature. Here, the $(CH_2)_2$ moiety of the linker is additionally oscillating back and forth between the imidazolate and the carboxylate group. The dry and the wet experimental spectra still show many similarities in region VII, suggesting that also the dried structure still could contain some crystal water consistent with the thermogravimetric investigations. The most obvious hint is the fact that the three lowest frequency peaks with the highest calculated IR activities in the shown spectra (animations at 571, 547, and 511 cm^{-1}) in the simulations nearly exclusively correspond to motions of the crystal water. In this region, both the dried and the wet samples show very similar spectral features.

In GUT2, the small peak labeled with the Roman number I (1661 cm^{-1}) corresponds to the (symmetric) bending mode of crystal water. This peak appears to disappear in the spectrum with heavy crystal water. A more in-depth analysis, however, shows that it is shifted to ≈1200 cm^{-1} (for details see discussion of measured and simulated vibrational properties of H_2O- and D_2O-containing systems in the Supporting Information). This shift is fully consistent with the experimental spectrum of the system with heavy crystal water, which shows an additional peak at ≈1200 cm^{-1} compared to the system with light water. The strong peak (region II) close to ≈1600 cm^{-1} corresponds to in-plane stretching of the COO^- groups (1594 and 1588 cm^{-1} consistent with the results for GUT1). Additionally, one notices small contributions of crystal water deformations. In the dried system, these additional oscillating masses are absent, thus, decreasing the effective mass and increasing the observed frequency.

This is seen in the increase of the experimentally determined frequency of the strong peak of the dehydrated system (1622 cm^{-1}) compared to the hydrated one (1599 cm^{-1}). Region III is characterized by several types of motions involving deformations of the 2-methyl-imidazolate moieties (1532–1408 cm^{-1}) with the lowest wavenumber ones predominantly involving the methyl group. Region III ends at the second highest peak (in the simulations), at 1383 cm^{-1}. Here, increasingly many C—H bending motions of the aliphatic backbones (CH_2 moieties) of the linkers are involved. Region III at 1384–1082 cm^{-1} is characterized by a mixture of deformation in the imidazole moieties together with CH bending motions and torsions in the residual linker. The situation changes to some extent below ≈1000 cm^{-1}, which marks the start of region V. In this region, one finds (in order of decreasing frequency) torsions of the methyl groups

EurJIC
European Journal of Inorganic Chemistry

Research Article
doi.org/10.1002/ejic.202500032

Chemistry
Europe
European Chemical
Societies Publishing

(998 and 952 cm^{-1}) and of the CH$_2$ groups in the aliphatic backbone of the linker (930 and 861 cm^{-1}). Although the latter are also partly present in the following region (region VI), this lowest wavenumber regime in the H$_2$O case comprises additional contributions due to the crystal water. Region VI starts with a mode (748 cm^{-1}) which shows a strong peak in the experimental spectra. The animations show that it mostly involves out-of-plane bending of the hydrogens of the imidazole moieties. Although the observed frequency of this mode (in the simulations and the experiments) for the wet crystals appears to be relatively independent of the hydrogen isotope in the crystal water, the mode appears to be notably shifted to higher frequencies for the dried sample in the experiments. The animation of this mode suggests an explanation for this observation: the moving hydrogen atoms are directed approximately toward the oxygen of one of the crystal water molecules. This suggests that the crystal water influences the (curvature) of the potential energy surface, such that the frequency decreases compared to the dehydrated case. This is most probably a consequence of the interaction of those hydrogens with the (partially negatively) charged oxygen of the crystal water softening the corresponding motion. The remaining modes in region VI (<729 cm^{-1}) appear in regions, where there are clear spectral features in all measurements. Most vibrations between ≈729 and ≈665 cm^{-1} strongly involve water vibrations. According to the simulations, these modes shift to much lower frequencies upon using deuterated crystal water (see Supporting Information). The shifted vibrational features come to lie outside the experimentally assigned spectral region. Thus, they cannot be identified as new peaks, which could be used for monitoring the drying process. To what extent features in the said spectral region diminish for deuterated crystal water is hard to tell due to the pronounced (water-) background at lower wavenumbers in the wet sample, but, overall, the main spectral features appear to prevail in the experiments (see also Supporting Information). Moreover, there are additional IR-active modes in that spectral region, which do not strongly involve crystal water. These, for example, include a stretching mode of the imidazole part at 721 cm^{-1} and similar distortions (633, 605, and 543 cm^{-1}) also including notable torsions in the aliphatic backbones.

Surface area determinations with GUT1-GUT3 were conducted in order to characterize the potential porosity of the samples. However, Brunauer–Emmett–Teller (BET) surface area measurements with nitrogen revealed a nonporous nature of all coordination polymers under investigation (nitrogen sorption resulted in surface areas typically below 10 m^2 g^{-1}). This behavior was attributed to the small diameter of the pores available in GUT1-GUT3 impeding the entrance of N$_2$ molecules (kinetic diameter of 3.64 Å). GUT2 was further tested for CO$_2$ (3.3 Å) and CH$_4$ (3.8 Å) uptake because similar Zn-based coordination polymers exhibited considerable CO$_2$ uptake and at the same time almost no uptake of N$_2$.[30,31] For that purpose, crystals of GUT2 were outgassed at 100 °C overnight prior to the measurements. The sorption capacities at 25 °C for both CO$_2$ and CH$_4$ yield values of 0.41 mmol g^{-1} and 0.17 mmol g^{-1} up to 30 bars (Figure S14, Supporting Information). In spite of the relatively low capacity, the methane isotherm tends to be of the Langmuir-type reaching sorption saturation at high pressures. CO$_2$ adsorption follows a
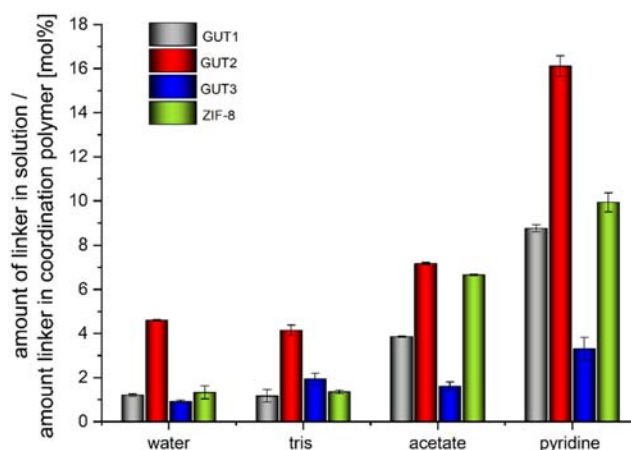

Figure 9. Share of GUT1-GUT3 and ZIF-8 dissolved in water and buffers (100 mM) made of tris(hydroxymethyl)aminomethane (HCl, pH 8.1), acetic acid/acetate (pH 4.7) and pyridine/(HCl, pH 5.2). The percentage is calculated by setting the amount of linker in solution in relation to the amount of linker in the coordination polymer used.

more linear trend (at least in the high-pressure region) indicating that CO$_2$ binds mainly on the surface of the particles in this regime. Adsorption isotherms up to 1 bar indicate a higher affinity for CO$_2$ capture with CO$_2$/CH$_4$ Ideal Adsorbed Solution Theory[32] selectivity of 3.5 at a partial pressure of 0.5 (Figure S15, Supporting Information). Nevertheless, the final uptakes are still quite low in comparison with common porous (or even nonporous like ZIF-4) imidazolate frameworks[33] suggesting that framework openings are not accessible for the gases under evaluation.

In the next step, the solubility of GUT1-GUT3 in water and different puffer solutions was studied in comparison to ZIF-8. For this purpose, the concentration of the free ligand in the supernate was determined after 24 h at room temperature and correlated with the amount of coordination polymer used. As shown in **Figure 9**, in water (as well as in all buffer solutions), the solubility of GUT2 is the highest compared to the other coordination polymers investigated. While the solubility in the Tris buffer is similar to that in water, the solubility in the acetate buffer is higher and the solubility in the pyridine buffer is highest. GUT3 is the least soluble coordination polymer in the latter two puffers and its solubility is significantly lower than that of ZIF-8,[34–36] especially in the acetate and pyridine buffers.

3. Conclusions

A resource-conserving two-step reaction sequence consisting of a solvent-free aza-Michael reaction of imidazole derivatives with methyl acrylate and concomitant saponification upon addition of aqueous sodium hydroxide afforded the desired analytically pure 3-(1H-imidazol-1-yl)propanoate linkers in virtually quantitative yields. These linkers were shown to form coordination polymers with Zn^{2+} salts upon combining aqueous solutions of the starting materials. In all coordination polymers, the coordination geometry of the zinc atoms is tetrahedral and each Zn atom is connected to two imidazole nitrogens and two carboxylate

EurJIC
European Journal of Inorganic Chemistry

Research Article
doi.org/10.1002/ejic.202500032

Chemistry Europe
European Chemical Societies Publishing

groups of four different linkers in κ^1-fashion. In the case of sodium 3-(1H-imidazol-1-yl)propanoate, the solid-state structure is characterized by the formation of a 2D network of the Zn ions and the linkers which are connected via crystal water chains forming a 3D network. In the case of 2-substituted 3-(1H-imidazol-1-yl)propanoate ligands, single polymer chains are formed that alternate along the b-axis of the crystal in the solid state. In the case of the 2-methylimidazol based linker, the chains are held together by hydrogen bonding of crystal water in the c-direction of the unit cell, while in the case of 3-(2-phenyl-1H-imidazol-1-yl)propanoate-based coordination polymers, no such water was found in the solid-state structure. All studied coordination polymers are thermally stable up to at least 200 °C. The imidazole and the 2-methylimidazol-based materials lose their crystal water and in the case of the latter material the crystalline order is not lost upon water removal. This effect was also studied by infrared spectroscopy and the assignment of the infrared spectra was accomplished with the help of density-functional theory-based calculations. The solubility of the coordination polymers in water and buffer solutions was investigated and compared with the solubility of ZIF-8. The highest solubility was found for the 3-(2-methyl-1H-imidazol-1-yl)propanoate-based coordination polymer, while the 3-(2-phenyl-1H-imidazol-1-yl)propanoate-based material showed the lowest solubility.

4. Experimental Section

Chemicals were purchased from Sigma–Aldrich, TCI, or ABCR and were used as received. The ligand precursors **3a–3e** were prepared according to the literature.[26] IR spectra were obtained with an Alpha FT-IR spectrometer from Bruker with the Platinum ATR single reflection diamond ATR module and analyzed using the Bruker Opus software. The TGA measurements were performed on a Netzsch STA 449 C. The purge and protective gases were helium, with a flow rate of 50 mL min^{-1} and aluminum crucibles were used. The temperature was increased with a heating rate of 10 °C min^{-1} from 20 to 550 C. The measurements of the sorption isotherms were done on an HTP IMI manometric gas sorption analyzer (Hiden Isochema Inc.). The ^{1}H and ^{13}C NMR spectra were recorded on a Bruker Ultrashield 300 operating at 300.36 MHz (^{1}H) and 75.53 MHz (^{13}C). Chemical shifts for the ^{1}H–spectra are reported in parts per million (ppm) relative to the singlet of CDCl$_3$ at 7.26 ppm or relative to the signal of D$_2$O at 4.79 ppm. The chemical shifts for the ^{13}C-spectra are reported relative to the CDCl$_3$ signal at 77.16 ppm. In the case of spectra recorded in D$_2$O, 2,2,3,3-D$_4$-3-(trimethylsilyl)propionic acid, sodium salt was used as the reference. Deuterated solvents and standards were obtained from Cambridge Isotope Laboratories Inc. The remaining peaks were identified according to the literature. The shape of the occurring peaks is specified as follows: s (singlet), d (doublet), t (triplet), and m (multiplet). X-ray powder diffraction (pXRD) profiles were measured with a Siemens D-5005 powder diffractometer with Bragg–Brentano geometry, operated at 400 kV and 300 mA, using Cu-K$_\alpha$ radiation, a graphite monochromator, and a scintillation counter. The step width was 0.02° with constant counting times of 20 s per step. Sc-XRD data collection was performed for GUT1-GUT3, on a Bruker APEX II diffractometer with the use of an Incoatec microfocus sealed tube of Mo K$_\alpha$ radiation ($\lambda = 0.71073$ Å) and a CCD area detector. Empirical absorption corrections were applied using SADABS or TWINABS.[37,38] The structures were solved with the use of the intrinsic phasing option in SHELXT and refined by the full-matrix least-squares procedures in SHELXL.[39–41] The space

group assignments and structural solutions were evaluated using PLATON.[42,43] Nonhydrogen atoms were refined anisotropically. All hydrogen atoms were located in a different map and refined isotropically. The carbon atoms of the phenyl group in GUT3 were disordered. Details of the crystal parameters, data collection, and refinements for complexes GUT1-GUT3 are summarized in **Table 1**. Bond lengths and angles as well as further details are given in the Supporting Information. Deposition Number(s) 2382832 (GUT1), 2382832 (GUT2), and 2382832 (GUT3) contain(s) the supplementary crystallographic data for this article. These data are provided free of charge by the joint Cambridge Crystallographic Data Centre and Fachinformationszentrum Karlsruhe (Access Structures service).

Synthesis of Sodium 3-(1H-Imidazol-1-yl)Propanoate (4a)

To methyl 3-(1H-imidazol-1-yl)propanoate (**3a**, 5.00 g, 32.43 mmol), an aqueous solution of NaOH (6.88 M, 4.7 mL, 1.02 eq.) was added in a glass vial. The resulting suspension was heated to 80 °C under stirring and kept at this temperature for 3 h, whereupon a clear solution formed. Volatiles were removed in a vacuum. Upon further drying in vacuum yellow crystals formed. Yield: 5.15 g (98%). Anal. calcd. for C$_6$H$_7$N$_2$O$_2$Na: C, 44.45; H, 4.35; N, 17.28; found: C, 44.26; H, 4.42; N, 17.02. ^{1}H-NMR (300 MHz, 25 °C, D$_2$O) $\delta = 7.66$, 7.15, 6.98 (s, 3H, Im^{2,4,5}), 4.24 (t, $J = 6.6$ Hz, 2H, NCH$_2$CH$_2$COO), 2.64 (t, $J = 6.6$ Hz, 2H, NCH$_2$CH$_2$COO) ppm. ^{13}C{^{1}H}-NMR (75 MHz, 25 °C, D$_2$O) $\delta = 182.2$ (COO), 140.8, 130.3 122.8 (Im^{2,4,5}), 47.0 (NCH$_2$CH$_2$COO), 41.6 (NCH$_2$CH$_2$COO) ppm. IR (ATR) $v = 3162$, 1575, 1510, 1441, 1407, 1377, 1085, 827, 751 cm^{-1}.

Synthesis of Sodium 3-(2-Methyl-1H-Imidazol-1-Yl) Propanoate (4b)

4b was prepared analogously to **4a**, using **3b** (4.74 g, 0.028 mol) as the starting material, and heating of the reaction mixture at 80 °C was carried out for 6 h. Yield: 4.83 g (98%), slightly yellow microcrystals. Anal. calcd. for C$_7$H$_9$N$_2$O$_2$Na: C, 47.73; H, 5.15; N, 15.90; found: C, 47.49; H, 5.46; N, 15.66. ^{1}H-NMR (300 MHz, D$_2$O) $\delta = 7.04$, 6.86 (s, 2H, Im^{4,5}), 4.15 (t, $J = 6.8$ Hz, 2H, NCH$_2$CH$_2$COO), 2.60 (t, $J = 6.9$ Hz, 2H, NCH$_2$CH$_2$COO), 2.35 (s, 3H, Im-CH$_3$) ppm. ^{13}C{^{1}H}-NMR (75 MHz, D$_2$O) $\delta = 182.1$ (COO), 148.7 (Im^2), 128.0, 123.0 (Im^{4,5}), 46.0 (NCH$_2$CH$_2$COO), 41.0 (NCH$_2$CH$_2$COO), 14.3 (Im-CH$_3$) ppm. IR (ATR) $v = 1600$, 1576, 1395, 1272, 676 cm^{-1}.

Synthesis of Sodium 3-(2-Phenyl-1H-Imidazol-1-Yl) Propanoate (4c)

4c was prepared analogously to **4a**, using **3c** (1.12 g, 5.2 mmol) as the starting material. Heating at 80 °C was done for 24 h. Yield: 1.20 g (97%). Anal. calcd. for C$_{12}$H$_{11}$N$_2$O$_2$Na: C, 60.50; H, 4.65; N, 11.76; found: C, 60.41; H, 4.82; N, 11.46. ^{1}H-NMR (300 MHz, D$_2$O) $\delta = 7.57$ (bs, 5H, Ph), 7.28, 7.09 (s, 2H, Im^{4,5}), 4.27 (t, $J = 7.0$ Hz, 2H, NCH$_2$CH$_2$COO), 2.56 (t, $J = 6.8$ Hz, 2H, NCH$_2$CH$_2$COO) ppm. ^{13}C{^{1}H}-NMR (75 MHz, D$_2$O) $\delta = 181.7$ (COO), 150.6 (Im^2), 132.6–124.3 (Ph), 128.1, 125.9 (Im^{4,5}), 46.7 (NCH$_2$CH$_2$COO), 41.1 (NCH$_2$CH$_2$COO) ppm. IR (ATR) $v = 1538$, 1479, 1457, 1408, 1367, 1248, 779, 728, 701 cm^{-1}.

Synthesis of GUT1

An aqueous solution of **4a** (10.0 mL, 0.1 mol L^{-1}) was prepared in a lockable reaction vessel, and an aqueous solution of Zn(NO$_3$)$_2$·6 H$_2$O (1.0 mL, 0.5 mol L^{-1}) was added, whereupon an oily precipitate formed. The locked reaction vessel was placed in an oven operated at 80 °C for 24 h, resulting in the formation of colorless crystals, which were collected on a glass frit and dried in vacuum at 80 °C for several days. Yield: 129 mg (75%). Anal. calcd. for C$_{12}$H$_{14}$N$_4$O$_4$Zn: C, 41.94; H,

Table 1. Crystal data and structure refinement for GUT1-GUT3; $R1 = \Sigma/|F_o| - |F_c|/|\Sigma|F_d$; $wR2 = [\Sigma_w(F_o^2 - F_2^2)^2/\Sigma_w(F_o^2)^2]^{1/2}$.

Formula	GUT1	GUT2	GUT3
	$C_{12}H_{14}N_4O_4Zn\cdot3(H_2O)$	$C_{14}H_{18}N_4O_4Zn\cdot H_2O$	$C_{24}H_{22}N_4O_4Zn$
F_w [g mol^{-1}]	397.69	389.73	495.82
a [Å]	11.7285(4)	15.1861(13)	8.3260(6)
b [Å]	8.2687(3)	15.0082(13)	15.9132(12)
c [Å]	17.4803(6)	15.0568(13)	17.4988(13)
α [°]	90	90	90
β [°]	90	90	102.110(3)
γ [°]	90	90	90
V [Å^3]	1695.23(10)	3431.7(5)	2266.9(3)
Z	4	8	4
Crytsal size [mm]	0.09 × 0.08 × 0.08	0.05 × 0.05 × 0.04	0.04 × 0.03 × 0.03
Crystal habit	Block, colorless	Block, colorless	Block, colorless
Crystal system	Orthorhombic	Orthorhombic	Monoclinic
Space group	Pca2$_1$	Pcca	P2/n
d_{calc} [mg m^{-3}]	1.558	1.509	1.453
μ [mm^{-1}]	1.49	1.46	1.12
T [K]	100(2)	100(2)	100(2)
2θrange [°]	2.3–32.8	2.7–33.2	2.4–32.6
F[000]	824	1616	1024
R_{int}	0.054	0.063	0.112
Independent reflections	6458	2995	5447
No. of parameters	297	298	428
R1, wR2 [all data][a]	R1 = 0.0242 wR2 = 0.0497	R1 = 0.0248 wR2 = 0.0568	R1 = 0.1074 wR2 = 0.2317
R1, wR2 [>2σ][b]	R1 = 0.0203 wR2 = 0.0482	R1 = 0.0212 wR2 = 0.0533	R1 = 0.0976 wR2 = 0.2274

4.11; N, 16.30; found: C, 41.22; H, 4.23; N, 16.11. IR (ATR) $v = 3112$, 1590, 1532, 1386, 1353, 1295, 1237, 1091, 950, 758, 650 cm^{-1}.

Similarly, GUT1 can be obtained from ethanolic or methanolic and from buffered solutions (Tris buffer, 100 mM). $Zn(NO_3)_2\cdot6\ H_2O$ can be replaced by zinc acetate.

Synthesis of GUT2

An aqueous solution of **4b** (5.0 mL, 0.156 mol L^{-1}) was prepared in a lockable reaction vessel, and an aqueous solution of $Zn(NO_3)_2\cdot6\ H_2O$ (5.0 mL, 0.079 mol L^{-1}) was added. Upon addition of the linker solution to the Zn-salt solution, immediate precipitation of a crystalline material was observed. Upon standing for 24 h at room temperature, bigger crystals were obtained, which were collected on a glass frit and dried in vacuum at 80 °C for several days. Yield: 143 mg (77%). Anal. calcd. for $C_{14}H_{18}N_4O_4Zn$: C, 45.24; H, 4.88; N, 15.07; found: C, 45.22; H, 5.02; N, 14.96. IR (ATR) $v = 3115$, 1625, 1392, 1296, 1279, 1009, 639 cm^{-1}.

Similarly, GUT2 can be obtained from ethanolic solution. $Zn(NO_3)_2\cdot6\ H_2O$ can be replaced by zinc acetate.

Synthesis of GUT3

GUT3 was prepared analogously to GUT1 using **4c** as the linker. Upon addition of the linker solution to the Zn-salt solution immediate formation of a cloudy material was observed. Upon heating to 80 °C

for 24 h, the cloudy material was contracted to a crystalline yellow solid, not suitable for single crystal X-ray diffraction. Recrystallization of the solid was observed by heating the material up to 150 °C for half an hour and in addition leaving it for 24 h at 80 °C. The formed single crystals were collected on a glass frit and dried in vacuum at 80 °C for several days. Yield: 139 mg (56%). Anal. calcd. for $C_{24}H_{22}N_4O_4Zn$: C, 58.14; H, 4.47; N, 11.30; found: C, 57.78; H, 4.72; N, 10.95. IR (ATR) $v = 3110$, 1624, 1450, 1386, 1364, 1309, 687 cm^{-1}.

Similarly, GUT3 can be obtained from ethanolic solutions.

Solubility Determination

Small amounts of the coordination polymers (GUT1-GUT3) (≈20 mg) were suspended in 1 mL water, a tris-, acetate-, or a pyridine buffer with a concentration of 100 mM, respectively. The mixtures were left at room temperature and after 24 h a part of the solution (100 μL) was taken off, evaporated, and dissolved in 600 μL deuterated water (D_2O). 100 μL of a standard solution (absolute ethanol in D_2O) was added and ^{1}H-NMR was performed. From the known concentration of the standard, the concentration of dissolved ligand was calculated by integration.

Simulation of the IR Spectra of GUT-1 and GUT-2 Crystals

IR absorption spectra were simulated using density functional theory employing periodic boundary conditions based on the unit cells of the wet materials. The Vienna Ab Initio Simulation Package (VASP)

EurJIC
European Journal of Inorganic Chemistry

Research Article
doi.org/10.1002/ejic.202500032

Chemistry Europe
European Chemical
Societies Publishing

(version 5.4.4)[44–47] was used with the PBE functional[48] combined with the D3-BJ a posteriori van der Waals correction.[49,50] To define the basis set, a converged plane wave energy cutoff of 800 eV was used together with converged $1 \times 2 \times 1$ and $1 \times 1 \times 1$ **k**-meshs for GUT-1 and GUT-2, respectively. The Phonopy[51] package was employed for simulating vibrational eigenfrequencies and dynamical matrices. The latter were combined with the Born effective charge tensors α[52–55] to obtain the IR intensities of the individual modes. The animations of the phonon modes were recorded by joining single pictures of geometries displaced along the eigenmodes using Ovito.[56] In the simulations, a perfectly crystalline sample consisting of isotropically aligned crystallites was assumed, which is not necessarily the case especially in ATR experiments in which only small sample volumes are probed. Therefore, calculated and measured peak intensities cannot be expected to match. Moreover, the physical nature of the evanescent wave is expected to trigger a minor redshift of ATR spectra compared, e.g., to IR transmission experiments.[57] Further details on the simulations can be found in the Supporting Information.

Acknowledgements

Conflict of Interest

The authors declare no conflict of interest.

Data Availability Statement

The data that support the findings of this study are available in the supplementary material of this article.

[1] H.-C. Zhou, J. R. Long, O. M. Yaghi, *Chem. Rev.* **2012**, *112*, 673.
[2] Q. Wang, D. Astruc, *Chem. Rev.* **2020**, *120*, 1438.
[3] D. Li, A. Yadav, H. Zhou, K. Roy, P. Thanasekaran, C. Lee, *Glob. Chall.* **2024**, *8*, 2300244.
[4] M. Moharramnejad, A. Ehsani, S. Salmani, M. Shahi, R. E. Malekshah, Z. S. Robatjazi, H. Parsimehr, *J. Inorg. Organomet. Polym. Mater.* **2022**, *32*, 3339.
[5] H. Li, M. Eddaoudi, M. O'Keeffe, O. M. Yaghi, *Nature* **1999**, *402*, 276.
[6] A. Phan, C. J. Doonan, F. J. Uribe-Romo, C. B. Knobler, M. O'Keeffe, O. M. Yaghi, *Acc. Chem. Res.* **2010**, *43*, 58.
[7] K. S. Park, Z. Ni, A. P. Côté, J. Y. Choi, R. Huang, F. J. Uribe-Romo, H. K. Chae, M. O'Keeffe, O. M. Yaghi, *Proc. Natl. Acad. Sci. U. S. A.* **2006**, *103*, 10186.
[8] M. Jian, B. Liu, R. Liu, J. Qu, H. Wang, X. Zhang, *RSC Adv.* **2015**, *5*, 48433.
[9] M. Bosch, M. Zhang, H.-C. Zhou, *Adv. Chem.* **2014**, *2014*, 1155.
[10] S. Hausdorf, J. Wagler, *J. Phys. Chem. A* **2008**, *112*, 7567.
[11] Y.-X. Sun, W.-Y. Sun, *CrystEngComm* **2015**, *17*, 4045.
[12] G. V. Scaeteanu, C. Maxim, R. Badea, R. Olar, *Molecules* **2023**, *28*, 1132.
[13] Y.-H. Xu, Y.-Q. Lan, X.-L. Wang, H.-Y. Zang, K.-Z. Shao, Y. Liao, Z.-M. Su, *Solid State Sci.* **2009**, *11*, 635.
[14] A. A. García-Valdivia, E. Echenique-Errandonea, G. B. Ramírez-Rodríguez, J. M. Delgado-López, B. Fernández, S. Rojas, J. Cepeda, A. Rodríguez-Diéguez, *Inorganics* **2021**, *9*, 20.
[15] S.-S. Chen, Q. Liu, Y. Zhao, R. Qiao, L.-Q. Sheng, Z.-D. Liu, S. Yang, C.-F. Song, *Cryst. Growth Des.* **2014**, *14*, 3727.
[16] Y. Zhang, Z. Du, X. Luo, *Z. Anorg. Allg. Chem.* **2015**, *641*, 2637.
[17] J.-L. Li, W.-D. Li, Z.-W. He, S.-S. Han, S.-S. Chen, *Crystals* **2018**, *8*, 424.
[18] P. Mahata, S. Natarajan, *Eur. J. Inorg. Chem.* **2009**, *11*, 2156.
[19] J.-F. Song, R.-S. Zhou, T.-P. Hu, Z. Chen, B.-B. Wang, *J. Coord. Chem.* **2010**, *63*, 4201.
[20] H.-W. Kuai, J. Fan, Q. Liu, W.-Y. Sun, *CrystEngComm* **2012**, *14*, 3708.
[21] Q. Zhai, R. Zeng, S. Li, Y. Jiang, M. Hu, *CrystEngComm* **2013**, *15*, 965.
[22] W.-Y. Yin, Z.-L. Huang, X.-Y. Tang, J. Wang, H.-J. Cheng, Y.-S. Ma, R.-X. Yuan, D. Liu, *New J. Chem.* **2015**, *39*, 7130.
[23] S.-S. Zhang, Y.-T. Yan, W.-Y. Zhang, Y.-K. Fan, Y. Zhang, K. Zhong, Y.-Y. Wang, *Inorg. Chim. Acta* **2019**, *495*, 118971.
[24] H.-J. Li, X.-Y. Zhang, K. Huang, D.-B. Qin, *Polyhedron* **2022**, *220*, 115850.
[25] M. B. Gawande, V. D. B. Bonifµcio, R. Luque, B. S. Branco, R. S. Varma, *ChemSusChem* **2014**, *7*, 24.
[26] K. Kodolitsch, F. Gobec, C. Slugovc, *Eur. J. Org. Chem.* **2020**, *19*, 2973.
[27] S. Lee, C. S. Poojari, A. Maznichenko, D. Roesel, I. Swiderska, P. Pohl, J. S. Hub, S. Roke, *J. Am. Chem. Soc.* **2024**, *146*, 19818.
[28] C. Healy, K. M. Patil, B. H. Wilson, L. Hermanspahn, N. C. Harvey-Reid, B. I. Howard, C. Kleinjan, J. Kolien, F. Payet, S. G. Telfer, P. E. Kruger, T. D. Bennett, *Coord. Chem. Rev.* **2020**, *419*, 213388.
[29] J. B. James, Y. S. Lin, *J. Phys. Chem. C* **2016**, *120*, 14015.
[30] Y.-M. Jeon, G. S. Armatas, J. Heo, M. G. Kanatzidis, C. A. Mirkin, *Adv. Mater.* **2008**, *20*, 2105.
[31] B. Chen, S. Ma, F. Zapata, F. R. Fronczek, E. B. Lobkovsky, H.-C. Zhou, *Inorg. Chem.* **2007**, *46*, 1233.
[32] N. F. Cessford, N. A. Seaton, T. Düren, *Ind. Eng. Chem. Res.* **2012**, *51*, 4911.
[33] J. McEwen, J.-D. Hayman, A. O. Yazaydin, *Chem. Phys.* **2013**, *412*, 72.
[34] M. A. Luzuriaga, C. E. Benjamin, M. W. Gaertner, H. Lee, F. C. Herbert, S. Mallick, J. J. Gassensmith, *Supramol. Chem.* **2019**, *31*, 485.
[35] M. D. J. Velásquez-Hernández, E. Astria, S. Winkler, W. Liang, H. Wiltsche, A. Poddar, R. Shukla, G. D. Prestwich, J. Paderi, P. Salcedo-Abraira, H. Amenitsch, P. Horcajada, C. J. Doonan, P. Falcaro, *Chem. Sci.* **2020**, *11*, 10835.
[36] M. D. J. Velásquez-Hernández, R. Ricco, F. Carraro, F. T. Limpoco, M. Linares-Moreau, E. Leitner, H. Wiltsche, J. Rattenberger, H. Schröttner, P. Frühwirt, E. M. Stadler, G. Gescheidt, H. Amenitsch, C. J. Doonan, P. Falcaro, *CrystEngComm* **2019**, *21*, 4538.
[37] Bruker: APEX2 and SAINT, *Bruker AXS Inc.*, Madison, Wisconsin, USA **2012**.
[38] R. Blessing, *Acta Crystallogr., Sect. A* **1995**, *51*, 33.
[39] G. M. Sheldrick, *Acta Crystallogr., Sect. A* **1990**, *46*, 467.
[40] G. M. Sheldrick, *Acta Crystallogr., Sect. A* **2008**, *64*, 112.
[41] G. M. Sheldrick, *Acta Crystallogr., Sect. A* **2015**, *71*, 3.
[42] A. L. Spek, *J. Appl. Cryst.* **2003**, *36*, 7.
[43] A. L. Spek, *Acta Crystallogr., Sect. D* **2009**, *65*, 148.
[44] G. Kresse, J. Hafner, *Phys. Rev. B* **1993**, *47*, 558.
[45] G. Kresse, J. Hafner, *Phys. Rev. B* **1994**, *49*, 14251.
[46] G. Kresse, J. Furthmüller, *Phys. Rev. B* **1996**, *54*, 11169.
[47] G. Kresse, J. Furthmüller, *Comput. Mater. Sci.* **1996**, *6*, 15.
[48] J. P. Perdew, K. Burke, M. Ernzerhof, *Phys. Rev. Lett.* **1996**, *77*, 3865.
[49] S. Grimme, J. Antony, S. Ehrlich, H. Krieg, *J. Chem. Phys.* **2010**, *132*, 154104.
[50] S. Grimme, S. Ehrlich, L. Goerigk, *J. Comput. Chem.* **2011**, *32*, 1456.
[51] A. Togo, I. Tanaka, *Scr. Mater.* **2015**, *108*, 1.
[52] J. M. Skelton, L. A. Burton, A. J. Jackson, F. Oba, S. C. Parker, A. Walsh, *Phys. Chem. Chem. Phys.* **2017**, *19*, 12452.
[53] D. Porezag, M. R. Pederson, *Phys. Rev. B* **1996**, *54*, 7830.
[54] P. Giannozzi, S. Baroni, *J. Chem. Phys.* **1994**, *100*, 8537.
[55] P. Brüesch, *Phonons: Theory and Experiments II*, Springer-Verlag, New York **1986**.
[56] A. Stukowski, *Model. Simul. Mater. Sci. Eng.* **2010**, *18*, 015012.
[57] T. G. Mayerhöfer, S. Pahlow, J. Popp, *ChemPhysChem* **2020**, *21*, 2029.
[58] K. Momma, F. Izumi, *J. Appl. Crystallogr.* **2011**, *44*, 1272.